sustainability

MDPI

Article

A Novel Approach for Secure Hybrid Islanding Detection Considering the Dynamic Behavior of Power and Load in Electrical Distribution Networks

Umme Kulsum Jhuma [1], Shameem Ahmad [1] and Tofael Ahmed [2,*]

[1] Department of Electrical Engineering, Faculty of Engineering, University of Malaya, Kuala Lumpur 50603, Malaysia
[2] Department of Electrical and Electronic Engineering, Chittagong University of Engineering & Technology, Chattogram 4349, Bangladesh
* Correspondence: tofael@cuet.ac.bd

Abstract: In the arena of modern electrical power distribution systems, distributed generators (DGs) are emerging as a manifestation of electric power personalization. Even though DGs have various advantages, unintentional islanding phenomena caused by DGs during abnormal grid operations can damage equipment connected to the grid. Therefore, islanding detection mechanisms are essential for DGs in grid-connected mode to disconnect the DG from the grid in case of grid abnormalities by obeying to specific grid codes. In this regard, a novel approach to develop a secure hybrid islanding detection method (IDM) is presented in this paper. The proposed hybrid IDM is developed by combining two passive IDMs known as rate of change of active power and rate of change of reactive power with an active IDM called load connecting strategy. An 11 kV Malaysian distribution system integrated with three types of DGs, namely synchronous generator, photovoltaic, and biomass, has been chosen as a testbed for the verification of the proposed hybrid IDM. Seven different case studies have been conducted in the PSCAD/EMTDC platform to validate the performance of the proposed IDM for islanding and non-islanding events. The simulation results confirm that the proposed IDM can detect islanding within 0.09 s, which is within 2 s complying with IEEE and IEC standards. Further, a comparative study based on the detection time and non-detection zone has been carried out, which has confirmed that the proposed IDM demonstrates better performance compared to the previously developed hybrid IDMs.

Keywords: islanding detection; synchronous generator; distributed generator; rate of change of power; non-detection zone

check for updates

Citation: Jhuma, U.K.; Ahmad, S.; Ahmed, T. A Novel Approach for Secure Hybrid Islanding Detection Considering the Dynamic Behavior of Power and Load in Electrical Distribution Networks. *Sustainability* **2022**, *14*, 12821. https://doi.org/10.3390/su141912821

Academic Editors: GM Shafiullah and Anis Zaman

Received: 9 November 2021
Accepted: 23 December 2021
Published: 8 October 2022

Publisher's Note: MDPI stays neutral with regard to jurisdictional claims in published maps and institutional affiliations.

Copyright: © 2022 by the authors. Licensee MDPI, Basel, Switzerland. This article is an open access article distributed under the terms and conditions of the Creative Commons Attribution (CC BY) license (https://creativecommons.org/licenses/by/4.0/).

1. Introduction

All over the world in recent times, the use of distributed generators (DGs) has increased in distribution networks due to their advantages such as cost-effective solutions to increasing load demand, peak shaving, improved power quality and reduced power losses to enhance the distribution system's reliability and performance [1,2]. Though DG has become an essential part of modern power system networks, during grid abnormalities (undervoltage and short circuit events), a DG needs to be detached from the grid for protection purposes by satisfying a set of grid standards produced by IEEE and IEC [3–5]. If the DG does not disconnect from the grid during unprecedented grid abnormality, then this phenomenon may lead to the damage of equipment connected to the grid and becomes a threat to the lives of distribution system line workers [6–8]. Therefore, to ensure the protection of DGs against unintentional islanding, islanding should take place to detach the DG from the grid within a specified time (seconds) using an autonomous disconnecting technique known as the islanding detection method (IDM). As per IEEE standard 1547, once islanding occurs, within 100 cycles or 2 s, it is mandatory for the DG to be detached from

the distribution network [3,4]. The importance of effective and quick detection of islanding for providing proper safety guidelines is mentioned extensively in IEEE Std.1547-2003, UL1741, IEC 62116 and IEEE Std. 929-2000 standards along with the value to be used in IDM [3–5,9,10].

IDM acts as an additional layer of protection for DGs by disconnecting them according to the grid integration standards to satisfy the local load during abnormal operation of the grid. During the abnormal operation/maintenance of the grid, this approach provides safe operation of the DGs and avoids complete blackout conditions [11,12]. Hence, fast and accurate detection of grid abnormality or islanding is essential. During this process, some challenges are faced by the DGs [6], which are:

- ➢ Due to the mismatch between supply and demand, the performance of DGs can be unstable.
- ➢ Due to unregulated islanding, distribution line maintenance staffs' lives may be at risk.
- ➢ After fault clearance, it is necessary to handle the resynchronization of DGs with the grid with safety regulation and extreme care.

Over the years, based on the aforementioned challenges and various grid standards, multiple IDMs have been proposed in the literature. A review of different types of IDMs along with their advantages and limitations, is presented in Table 1. The IDMs are broadly classified into two categories, namely remote and local methods, based on their location and the parameters used for their operation [13]. Remote IDMs are one of the most efficient and reliable methods as the DGs are directly communicating with the utility. A few of the most commonly implemented IDMs are power line carrier (PLC), phasor measurement units (PMU) and transfer trip [14–18]. The limitation of these remote IDMs is their complexity in implementation and cost during the setup stage [14,18].

Table 1. Overview of different IDMs.

Method	Advantage	Disadvantage	References
Remote IDMs			
Power line carrier	Real-time communication makes this method most accurate and reliable	Maintenance and implementation cost are very high.	[14,15]
Phasor Measuring Units	Detection process does not require any extra device, so it is easy to implement	Shows less robustness to handle different types of signals across the network.	[16,17]
Transfer Trip	It is a very simple concept to implement with a very small NDZ.	Maintenance and implementation cost are very high.	[18]
Active IDMs			
Active and Reactive Power Injection	The detection accuracy is high due to the injection of powers.	The voltage at distribution side rises which is a concern.	[19]
Active Frequency Drift	Balanced islanding conditions and small NDZ can be achieved.	Power quality degrades.	[20]
Impedance Measurement	The method operates well because of the absence of NDZ	This method is not suitable for parallel inverter connection.	[21]
Harmonic Signal Injection	During islanding, power balance can be achieved among generator and demand.	Detection time is high.	[22]
Slip Mode Frequency Shift	This method has small NDZ.	Inaccurate in measurement due to the presence of phase shift parabola	[23]
Sandia Frequency Shift (SFS)	Implementation is easy due to having very small NDZ.	Power system stability and quality are the concerns.	[24]
Sandia Voltage Shift	Islanding detection speed is fast.	Power quality and transient response of the system get affected.	[25]

Table 1. *Cont.*

Method	Advantage	Disadvantage	References
Frequency Jump	Effective for non-parallel multi DGs.	Less efficient for parallel DGs.	[26]
Virtual Capacitor and Inductor	Harmonics are lower at the output.	Power quality degrades.	[27]
Passive IDMs			
Rate of change of Power (ROCOP)	Suitable for large power mismatch.	Selection of threshold values are difficult.	[28,29]
Rate of change of Frequency (ROCOF)	Islanding detection speed is fast.	For small DGs, threshold values can be chosen accurately but for medium and large DGs it is difficult.	[30]
Over/Under Voltage and Frequency	Low cost and implementation is easy.	Due to large NDZ, detection time is long.	[31]
Change of Impedance	Suitable for small, medium and large DGs with large power mismatch.	Initialization of unwanted tripping is a concern.	[32]
Voltage Unbalance	It can easily identify unbalance in the 3-phase system.	For a single-phase system, it is not suitable.	[33]
ROCOF over ROCOP	Small power mismatch can be detected between load and DG	Threshold selection can cause incorrect detection.	[34]
Phase Jump	Implementation is easy.	When the DG meets local demand, it fails to detect islanding condition.	[35]
Hybrid IDMs			
Voltage and Reactive Power Shift	Fault tolerant capacity and robustness of the system improved.	Power system stability and quality are the concerns.	[36]
SFS and Q-f Based Scheme	Voltage regulation, and power factor improved.	Selection of threshold values are difficult and power quality degrade.	[37]
Positive Feedback and voltage unbalance	Tripping rate and false detection can be reduced.	For a single-phase system, it is not suitable.	[38]
SFS and ROCOF	Suitable for multi-DG system along with high accuracy and fast detection.	Sometimes allocation of trip boundary is tricky.	[39]
Rate of change of reactive power (ROCORP) and load connecting strategy (LCS)	It has fast detection speed.	Power system stability and quality are the concerns.	[40]
ROCOF over ROCORP	Fast detection speed with high accuracy.	Selection of threshold values are difficult.	[41]
Combined rate of change of voltage (ROCOV) and ROCORP	Small mismatch in power between DG and load can be easily detected.	Power system stability and quality are the concerns.	[42]
Rate of change of regulator voltage (ROCRV) over ROCORP	It can easily detect small mismatch in power among DGs and load.	Selection of threshold values are difficult.	[43]
Intelligent IDMs			
Fuzzy Logic	Suitable for multi-inverter-based DG system. It has good accuracy.	The results are dependent on a set of predefined rulesets.	[44]
Adaptive network-based fuzzy inference system (ANFIS)			[45]

Table 1. *Cont.*

Method	Advantage	Disadvantage	References
Artificial Neural Network (ANN)	Suitable for multi-DG system along with high accuracy and fast detection.	Implementation and computation are difficult because of requirement of large database for training.	[46]
Support Vector Machine (SVM)			[47]
Decision Tree			[48]
Signal Processing IDMs			
Wavelet Transform	It can operate in different bands of resolution due to variable size time frequency window.	Highly sensitive to noise signals. Computation time is very high.	[49]
S-Transform	Due to combined frequency-dependent time, space and referenced local phase information, accuracy is good.	Computation time is very high.	[50,51]
Mathematical Morphology	Through time-domain analysis, the noise in the data can be filtered.	Suitable only for single direction features and for randomly oriented features, it is not suitable. Computation time is very high.	[52]
Hilbert–Haung Transform	Suitable for both nonlinear and nonstationary data analysis.	The method cannot disintegrate numerically for components which have frequency proportions near to unity. Implementation is difficult.	[53]
Principle Component Analysis	Reduces data overfitting, removes correlated features, and improves visualization of data.	Information can be lost due to less interpretation of independent variables.	[54]
Gauss-Newton Algorithm	Due to tidy error estimates, the accuracy is high.	High computation time and implementation cost is also high.	[55]
Phaselet Algorithm	Fast estimation can be achieved by calculating the phasor of variable data.	Due to variable window size unwanted classification occurs during transients.	[56]

To overcome the problems associated with remote IDMs, local IDMs are introduced, which are categorized into active and passive methods. There are several active IDMs proposed in the literature [19–27], which are shown in Table 1. Though for active IDMs, non-detection zones (NDZ) are very small, the power quality of the network is affected due to the injection of disturbance into the system, and their islanding detection speed is slower than passive IDMs [20,22–25]. On the other hand, passive IDM is one of the most cost-effective IDMs as the different operating parameters (power, frequency, voltage, current, harmonic distortion, etc.) are measured at the point of common coupling (PCC) to identify the abnormalities in the system [31]. These methods can be applied to both meshed and radial distribution networks consisting of DGs because no disturbance is created by them in the network and they have a faster detection speed than active ones [35]. The shortcoming of these methods is that they have a large NDZ range, in which it is not possible to detect islanding, because any islanding occurrence disturbed signal cannot be recognized by passive IDMs in that range [31].

By combining different active and passive IDMs with each other or with signal processing and artificial intelligence-based IDMs, another method known as hybrid IDMs has been developed to address the problems of passive and active IDMs. These methods have small NDZ and, due to combined characteristics, they can improve the robustness and fault tolerant nature of the distribution network [36]. In addition, this IDM has high accuracy and a fast detection time [39]. However, power quality and system stability remain an issue

for this IDM [36,39]. Further, due to the combined feature, the islanding detection time of hybrid IDMs is higher than independent passive and active IDMs [40,42].

All the IDMs discussed earlier either depend on the sensors' pre-defined data limits or on the real-time data, even though most of the time they are accurate, but at certain anomalies, the pre-set data may not be sufficient, and this may lead to an unintended trip [6]. Therefore, advanced IDMs, namely intelligent and signal-processing IDMs, were introduced to overcome the issues of conventional IDMs. The advantages of intelligent IDMs over signal processing IDMs are high precision, good reliability, and a non-requirement of threshold value selection [49]. Even though intelligent IDMs can be easily implemented in an SG-based distribution system, in an inverter-based distribution system, they may not successfully detect islanding [44]. On the other hand, signal processing-based IDMs have a smaller NDZ compared to intelligent IDMs. The common drawbacks of both these methods are high computation and implementations are difficult [48,51].

It can be summarized from the earlier discussion that various methods of IDMs have been developed for detecting islanding efficiently and cost effectively. Nevertheless, these methods still have some limitations, such as complications in implementing the algorithm of IDM, a higher cost associated during the implementation of IDM, higher computation and detection time of the IDM algorithm, higher cost for maintenance and lack of implementation by considering a real-world power system network. As a result, robust IDM development with a simple algorithm and faster response is necessary, which could detect islanding within very short time. In addition, developed IDMs also have less implementation complexity for a practical power system network with a lower NDZ range. In [57], a hybrid method by combining ROCOP and LCS is proposed, which shows a faster detection time. However, the analysis of NDZ for IDM was not considered is this study. This paper aims to present a novel hybrid IDM to detect islanding conditions of DGs, namely a synchronous generator (SG), photovoltaic (PV) generator, and biomass generator. This paper considers a low-voltage distribution system of Malaysia with an 11 kV distribution voltage to evaluate the performances of the proposed hybrid IDM. A combination of two passive IDMs, namely ROCOAP and ROCORP, along with an active LCS method is considered in the proposed novel hybrid IDM. LCS works as active method because LCS checks the necessity of islanding by injecting extra amounts of load to the distribution system. Both the passive IDMs of ROCOAP and ROCORP are considered due the sensitivity of changing the reactive power in the system, as the reactive power changes might cause false islanding detection. Sometimes, IDM fails to detect islanding and non-islanding mode with the small changes in the system's reactive power demand, which might cause inappropriate disconnection of DGs from the distribution network. For this reason, the proposed IDM considers the combination of ROCOAP and ROCORP for proper distinguishing between the necessity of the true islanding state and the false islanding state. The proposed hybrid IDM has a fast islanding detection response as it contains the high-speed passive IDMs. This IDM, with a small detection time and small NDZ, is satisfactory for both multiple DGs and single synchronous DG. In addition, the proposed IDM can also avert short circuit fall. On top of this, the proposed IDM is simple and can be easily implemented in real-world distribution networks in comparison with common passive and active IDMs.

The main contributions of this paper are as follows:

- A hybrid IDM has been modelled and developed based on the combination of two passive IDMs, namely ROCORP and ROCOAP, and LCS as an active IDM to detect islanding phenomena at PCC.
- The proposed IDM's performance has been validated in a PSCAD environment for various cases, such as islanding, fault analysis, quality factor, load variations, DG tripping, power mispatch and NDZ range.
- The proposed IDM is applied at a PCC between DGs and an existing 11 kV Malaysian distribution network, which are modelled using the modules available from the PSCAD library.

➢ Finally, a comparative study has been conducted based on islanding detection time and NDZ to prove the better performance and effectiveness of the proposed IDM.

The organization of the paper is as follows: the proposed IDM's detailed modelling is presented in Section 2. In Section 3, the proposed IDM's NDZ range is presented. The details of the testbed are presented in Section 4. Section 5 presents the simulation results and analysis of the study along with the comparative study. Finally, in Section 6, the outcome of the research is summarized.

2. Modelling of Proposed Hybrid Islanding Detection Strategy

Active power and reactive power of DGs are represented in Equations (1) and (2), respectively. Here, the active power and reactive power of the grid, load and DGs are considered.

$$P_{DG} = R_L \times I_L + R_{DG} \times I_{DG} - \Delta P \tag{1}$$

$$Q_{DG} = X_L \times I_L + X_{DG} \times I_{DG} - \Delta Q \tag{2}$$

In Equation (1), P_{DG} is active power at the DG side, R_L is load resistance, I_L is load current, R_{DG} is DG resistance, I_{DG} is the current of the DG, and ΔP is active power difference of load and DG. In Equation (2), Q_{DG} is reactive power at the DG side, X_L is load reactance, I_L is load current, X_{DG} is reactance of DG, I_{DG} is the current of DG, and ΔQ is the reactive power difference of load and the DG.

This new hybrid method combines power change variations with the connected load variations to obtain the final result, which triggers the output signal for the breakers.

2.1. Active Power Method

One of the examples of passive IDM is the active power method. In this case, the power of a three-phase system is measured at PCC and is given by Equation (3).

$$P_{DG} = V_a I_a \cos\theta_a + V_b I_b \cos\theta_b + V_c I_c \cos\theta_c \tag{3}$$

The phase values of the output voltages are V_a, V_b, and V_c and the phase values of the output currents are I_a, I_b, and I_c. The system will not be islanded when the values of ROCOAP are lower than the threshold point, and at that time, the DGs will be connected with the grid. However, the system will operate in islanding mode while the values of ROCOAP are more than the threshold point. The values of ROCOAP can be obtained by differentiating Equation (3). During the islanding operation mode, the change in the ROCOAP value is significant. IDM modules send signals to DG breakers for disconnecting the DGs by observing the ROCOAP value. When the load's required power matches the supplied power by the DG, fewer oscillations are observed in the output, and for this, the IDM sometimes gives the wrong results. Hence, investigating this phenomenon is necessary to improve the IDM.

2.2. Reactive Power Method

The reactive power method is another passive IDM which is like the active power method, except for the sensitivity of ROCORP. The sensitivity of ROCORP is higher than the sensitivity of ROCOAP. System reactive power is monitored continuously for ROCORP. The reactive power equation of ROCORP at the PCC is given by Equation (4).

$$Q_{DG} = V_a I_a \sin\theta_a + V_b I_b \sin\theta_b + V_c I_c \sin\theta_c \tag{4}$$

The values of ROCORP can be obtained at PCC by differentiating Equation (4). While the system is connected to the grid, the oscillation does not cross the threshold point, but it crosses the threshold during islanding, and this is similar to ROCOAP.

2.3. IDM Final Stage including ROCOAP, ROCORP and LCS

Three different IDMs are considered to develop the hybrid IDM in this paper. The step-by-step process of implementing these three IDMs is depicted in Figure 1. From the figure, it can be seen that in the beginning, the module first considers active and reactive power responses from the DG side and compares the dataset with the margin limit. If the data cross the margin limit, then the module sends a positive signal to the breakers to trip. The breakers will receive the positive signal when Equations (9) and (14) are veracious.

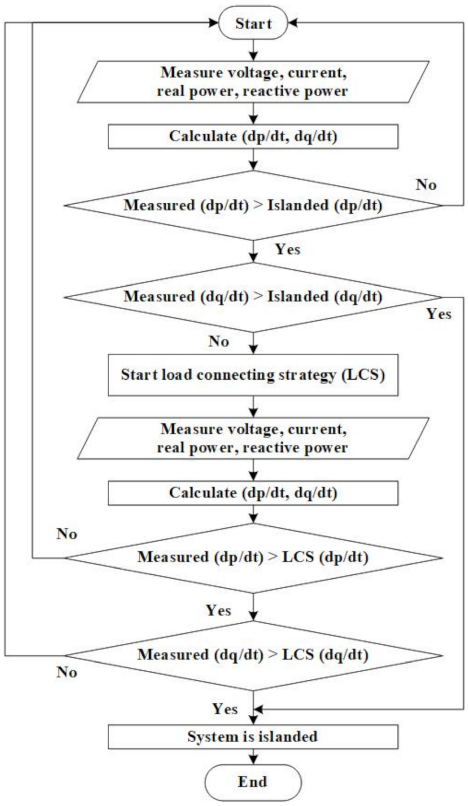


Figure 1. Illustration of the proposed algorithm's flowchart for hybrid IDM.

First stage: Given equations are the steps for the flowchart algorithm. Based on these equations, the module will work.

$$p = \left\{ p_{measured_i}, p_{measured_{i+1}}, p_{measured_{i+2}} \cdots\cdots\cdots\cdots\cdots p_{island} \right\} \tag{5}$$

$$q = \left\{ q_{measured_i}, q_{measured_{i+1}}, q_{measured_{i+2}} \cdots\cdots\cdots\cdots\cdots q_{island} \right\} \tag{6}$$

First step: $dp = dp_{measured_i}$, $dq = dq_{measured_i}$

$$\left(\frac{dp_{measured_i}}{dt} \right) > \left(\frac{dp}{dt} \right)_{Island} \tag{7}$$

If Equation (7) is not true, then

$$dp = dp_{measured_{i+1}} \left(\frac{dp_{measured_{i+1}}}{dt} \right) > \left(\frac{dp}{dt} \right)_{Island} \tag{8}$$

If Equation (8) is true, then

$$dq = dq_{measured_i} \left(\frac{dq_{measured_i}}{dt} \right) > \left(\frac{dq}{dt} \right)_{Island} \tag{9}$$

If Equation (9) is true, then the system is islanded. If it is not true, then the LCS will be initiated.

At a specific time, $(dp/dt)_{measured}$ and $(dq/dt)_{measured}$ are the values of ROCOAP and ROCORP, respectively, received by the module. $(dp/dt)_{Island}$ and $(dq/dt)_{Island}$ are the margin values which specify the data crossing limit for the islanding scenario. If reactive power is not more than the reference threshold value, then in the second stage, the LCS is connected for further clarification of islanding and non-islanding events, such as when there is an increase in total load, but the grid is still connected, or any induction motor has started or any capacitor bank is connected. When the power imbalance between the generation and demand is small, the LCS is connected. To accelerate the power change, a suitable value of R-L load is connected. The LCS will be activated when Equation (9) is not satisfied.

Second stage:

$$p = \left\{ p_{measured_i}, p_{measured_{i+1}}, p_{measured_{i+2}} \cdots\cdots\cdots\cdots\cdots p_{island,LCS} \right\} \tag{10}$$

$$q = \left\{ q_{measured_i}, q_{measured_{i+1}}, q_{measured_{i+2}} \cdots\cdots\cdots\cdots\cdots q_{island,LCS} \right\} \tag{11}$$

First step: $dp = dp_{measured_i}$, $dq = dq_{measured_i}$

$$\left(\frac{dp_{measured_i}}{dt} \right) > \left(\frac{dp}{dt} \right)_{Island,LCS} \tag{12}$$

If Equation (12) is not true, then

$$dp = dp_{measured_{i+1}} \left(\frac{dp_{measured_{i+1}}}{dt} \right) > \left(\frac{dp}{dt} \right)_{Island,LCS} \tag{13}$$

If Equation (13) is true, then

$$dq = dq_{measured_i} \left(\frac{dq_{measured_i}}{dt} \right) > \left(\frac{dq}{dt} \right)_{Island,LCS} \tag{14}$$

where $(dp/dt)_{Island,LCS}$ and $(dq/dt)_{Island,LCS}$ are the ROCOAP and ROCORP threshold values, respectively, after activating LCS.

If $(dp/dt)_{measured}$ is greater than the threshold $(dp/dt)_{Island,LCS}$, then the module will check the condition of Equation (14). If Equation (14) is not true, then the calculation will start back from the first stage where $dq = dq_{measuredi+1}$. On the contrary, if Equation (14) is true, circuit breakers will receive the signal to ensure the islanding by disconnecting the DGs.

The verification of the whole process has been carried out in a PSCAD/EMTDC simulation environment while the IDM module is developed using the FORTRAN language. The required real and reactive power of the load can be calculated using Equations (15) and (16). Islanding will be detected by the module based on the comparison of active and reactive power responses and LCS together.

$$P_{load} = P + \Delta P \tag{15}$$

$$Q_{load} = Q + \Delta Q \tag{16}$$

where P_{load} and Q_{load} are the load's real and reactive powers, respectively. ΔP and ΔQ are the changes in real and reactive power, respectively. P and Q are the total active and reactive powers of the DGs, respectively.

The amplitude of the RLC load, including phase angle (ϕ_{LOAD}), resonant frequency (f_0) and the quality factor (Q_f), are given by Equations (17)–(20), respectively.

$$|\,z\,| = \frac{1}{\sqrt{\frac{1}{R^2} + \left(\frac{1}{\omega L} - \omega C\right)^2}} \tag{17}$$

$$\phi_{LOAD} = \tan^{-1}\left[Q_f\left(\frac{f_0}{f} - \frac{f}{f_0}\right)\right] \tag{18}$$

$$f_0 = \frac{1}{2\pi\sqrt{LC}} \tag{19}$$

$$Q_f = R\sqrt{\frac{C}{L}} \tag{20}$$

3. Non-Detection Zone (NDZ) of the Proposed Method

In dictating the precision and potency of the IDM, the NDZ plays an indispensable role. The NDZ represents the area or zone or the region in which the IDM will not be proficient enough to perceive islanding. It can be represented as a gap between the power supplied by the grid and the required resistive, capacitive or inductive load by consumers. The smaller the region of the NDZ, the more precise the IDM is.

The active power for NDZ can be calculated using Equation (21) [40]:

$$\Delta P = -3V \times \Delta V \times I \tag{21}$$

where ΔP = change in active power, V = estimated voltage, I = estimated current and ΔV = difference between voltage upper limit and lower limit.

The reactive power equation for NDZ is given by (22) [40]:

$$\Delta Q = 3\frac{V^2}{\omega_n L}\left(1 - \frac{f_n^2}{(f_n \pm \Delta f)^2}\right) \tag{22}$$

$$\omega_n = 2\pi f \tag{23}$$

$$L = \frac{V^2}{2} \times \pi \times f \times Q_f \times P \tag{24}$$

where ΔQ = change in reactive power, V = estimated voltage, f_n = nominal frequency, Δf = difference between frequency upper limit and frequency lower limit and Q_f = quality factor.

Equations (21) and (22) can also be represented as Equations (25) and (26), respectively.

$$\left(\frac{V}{V_{\max}}\right)^2 - 1 \le \frac{\Delta P}{P} \le \left(\frac{V}{V_{\min}}\right)^2 - 1 \tag{25}$$

$$Q_f \times \left(1 - \left(\frac{f}{f_{\min}}\right)^2\right) \le \frac{\Delta Q}{Q} \le Q_f \times \left(1 - \left(\frac{f}{f_{\max}}\right)^2\right) \tag{26}$$

where f = estimated frequency, V = estimated voltage, P = active power, Q = reactive power, Q_f = quality factor, ΔP = change in active power, ΔQ = change in reactive power, V_{max}, V_{min} = upper limit and lower limit of voltage and f_{max}, f_{min} = upper and lower limit of frequency.

For this study, the maximum and minimum values of the rated voltage are $V_{\max}$= 115% and $V_{\min}$= 85%, and maximum and minimum values of the frequency are $f_{\max}$= 51.5 Hz and $f_{\min}$= 48.5 Hz, and a quality factor Q_f = 2.5 is considered according to the IEC 62116 standard [5].

$$-24.39\% \le \frac{\Delta P}{P} \le 38.41\% \tag{27}$$

$$-15.7\% \leq \frac{\Delta Q}{Q} \leq 14.35\% \tag{28}$$

According to IEC 62116, the NDZ region for an active and reactive power imbalance of the distribution system should be in between (0.3841 MW to −0.2439 MW) and (0.1435 MVar and −0.1570 MVar), respectively [5]. The NDZ region for the proposed hybrid IDM is depicted in Figure 2. From Figure 2, it is observed that the proposed technique works efficiently when the real power imbalance is between 0.043 MW and −0.05 MW and the reactive power imbalance is between 0.043 MVar and −0.045 MVar. Thus, the proposed IDM increases the accuracy and also reduces the NDZ.

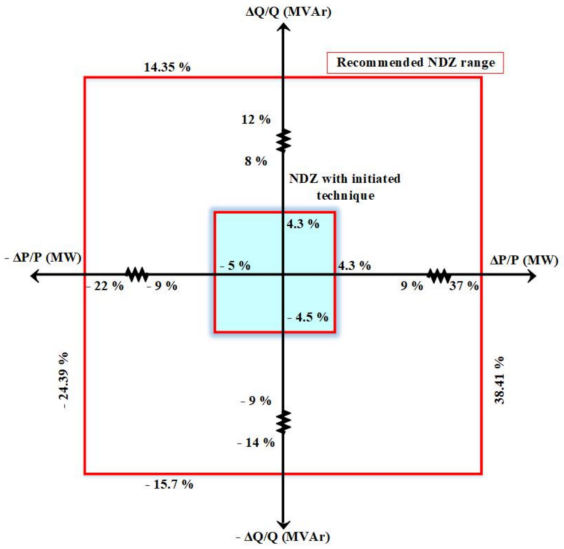


Figure 2. NDZ of the proposed islanding detection method.

4. Testbed under Study

The effectiveness of the proposed IDM mode is tested in this study by developing an 11 kV distribution system that is symmetrical with the Malaysian distribution system. The developed system consists of a synchronous generator (SG), a photovoltaic (PV) generation system, a biomass generator, 32 buses including DG buses, and 29 loads, including LCS. The testbed along with the DGs is modelled in the PSCAD environment. The modelling of the SG, PV and biomass systems is adopted from [40,58,59]. Figure 3 shows the test frame satisfying the IDM operations as per the IEEE 1547 standard recommendations and Figure 4 shows the developed system as per the IEEE 1547 standard. It can be seen from Figure 4 that the grid and LCS breakers can initiate islanding and LCS, respectively, in the testbed system. In addition, the connected load can be designed as various types, such as parallel RLC load, as the IDM performance depends on the load type. It can be concluded from Figure 4 that the developed system considers all the possible considerations mentioned in the IEEE 1547 standard.

The values of R, L and C loads can be calculated using Equations (29)–(31) when the power factor is equal to 1 [40]:

$$R = \frac{V^2}{P} \tag{29}$$

$$L = \frac{V^2}{2 \times \pi \times f \times Q_f \times P} \tag{30}$$

$$C = \frac{Q_f \times P}{2 \times \pi \times f \times V^2} \tag{31}$$

where Q_f = quality factor.

Values of loads can be calculated by using Equations (32)–(35) when the power factor is not equal to 1 [40]:

$$L = \frac{X_L}{2 \times \pi \times f} \tag{32}$$

$$X_L = \frac{V^2}{Q} \tag{33}$$

$$C = \frac{1}{2 \times \pi \times f \times X_C} \tag{34}$$

$$X_C = \frac{V^2}{Q} \tag{35}$$

where X_L and X_c are the inductive and capacitive reactances.

Tables A1 and A2 (Appendix A) exhibit the SG, transformer, PV, biomass and load data of an 11 KV Malaysian distribution system. The operating voltage of the SG and biomass is 3.3 KV, and for PV it is 0.23 kV. A step-up transformer rated at 2 MVA is connected to the DG units to step the voltage up to 11 kV. Three DG units supply 3.6 MW and 1.3 MVar power to the load.

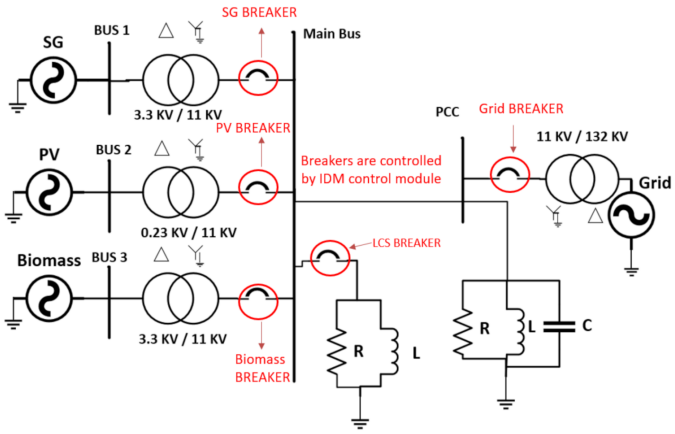


Figure 3. IEEE1547 test frame [40].

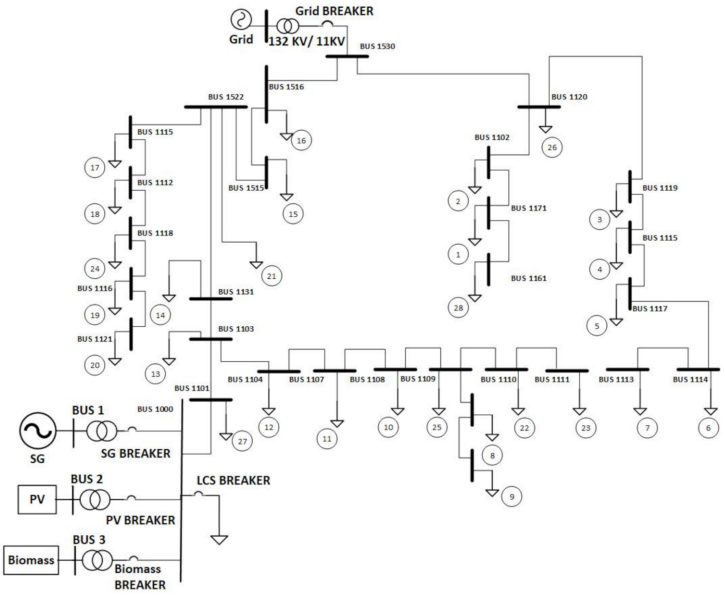


Figure 4. A 27 Bus Malaysian distribution network [40].

5. Simulation Results

Various cases including voltage and frequency variations have been considered to verify the performance of the proposed IDM on the PSCAD platform in an 11 kV, 27 bus Malaysian distribution system. Seven case studies are considered to examine the performances of the module under islanding and non-islanding cases to see whether the module can identify islanding cases as islanding and non-islanding cases as non-islanding, or mistakenly take a non-islanding as islanding. The threshold values were set according to the distribution system and DG responses. The module compares the instantaneous result with the given threshold to check the difference that occurs when the system enters the islanding mode, or in the case of other phenomena.

5.1. Case 1: Grid Supply Disconnected for Intentional Islanding Operation

Intentional islanding of the grid was performed by disconnecting the grid circuit breaker (CB) to check the module's functionality against the islanding detection, which is shown Figure 5. It can be seen from Figure 5 that the DG with the distribution network falls under the islanding condition due to the disconnection of the grid at t = 3 s. Figure 5 also shows that at t = 3.04 s, dp/dt reaches 4 MW/s, crossing the margin limit of 0.8 MW/s. Now, the module will measure ROCORP according to the flowchart in Figure 1, and the ROCORP DGs at PCC are shown in Figure 6. It can be seen from Figure 6 that the value of dq/dt crosses the margin of 0.019 MVar/s at t = 3.03 s. Therefore, the signal for disconnection of the DGs are sent to all DG breakers, as at t = 3.07, the islanding detection conditions are true. The real power and reactive power of DGs are depicted in Figure 7 at the time of islanding detection.

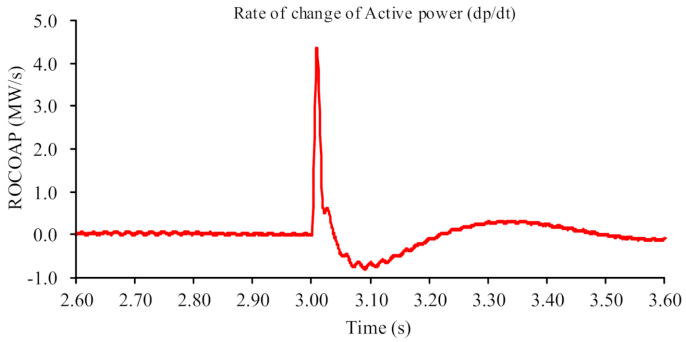


Figure 5. At PCC, DG's ROCOAP (dp/dt).

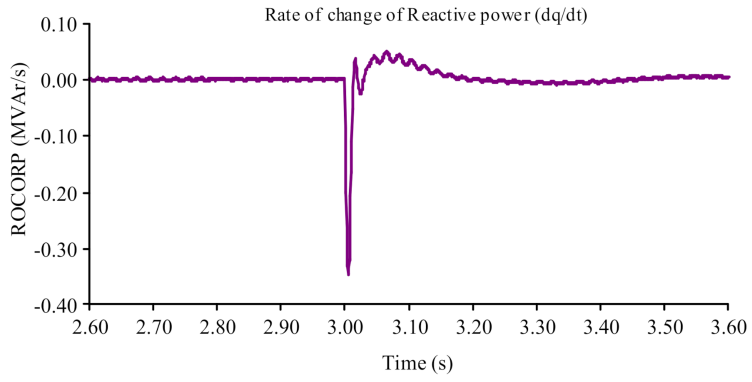


Figure 6. At PCC, DG's ROCORP output (dq/dt).

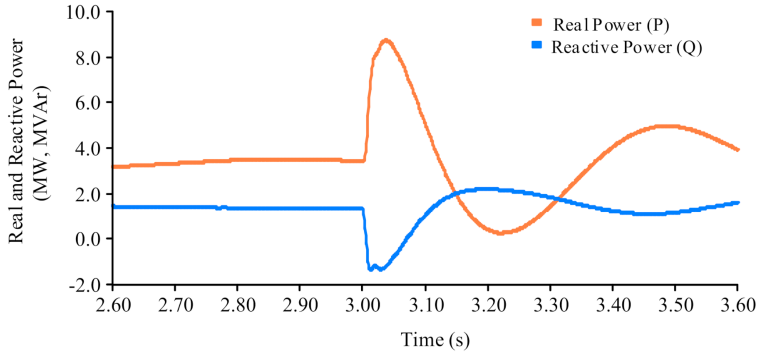


Figure 7. At PCC, DG's real and reactive power.

5.2. Case 2: Varying Quality Factors

The performance of the developed IDM was carried out by varying the quality factors (Q_f) according to IEEE Std. 929, IEEE Std. 1547, and UL1741 Std. Various standards encourage different values of quality factors; for example, in the IEEE Std. 1547, the value of Q_f = 1, while in the IEEE Std. 929, the value of Q_f is ≤2.5, and in the UL1741 Std. the recommended value of Q_f is ≤1.8. All these three standards' recommendations are considered while choosing the Q_f values to evaluate the developed IDM performance. The corresponding values of *R*, *L*, and *C* for different Q_f values are shown in Table 2. As shown in Figure 8, the value of ROCOAP drastically increases at t = 3 s, when DGs entered the islanding mode. After that, when the system checks the ROCORP, from Figure 9 it can be seen that it also crosses the threshold, thus detecting islanding within 0.08 s. Figure 10 represents PCC reactive and real power responses.

Table 2. Values of *R*, *L*, and *C* for different values of Q_f with proposed IDM's responses.

Quality Factor (Q_f)	*R* (Ω)	*L* (H)	*C* (F)	$\left(\frac{dp_{measured_i}}{dt}\right)$ (MW/s)	$\left(\frac{dq_{measured_i}}{dt}\right)$ (MVar/s)	Time (s)
1.8	2.304	0.00304	0.00231	0.30	0.15	3–3.08
2.5	2.304	0.00244	0.00231	0.28	0.19	3–3.02
3	2.304	0.00203	0.00288	0.20	0.08	3–3.05

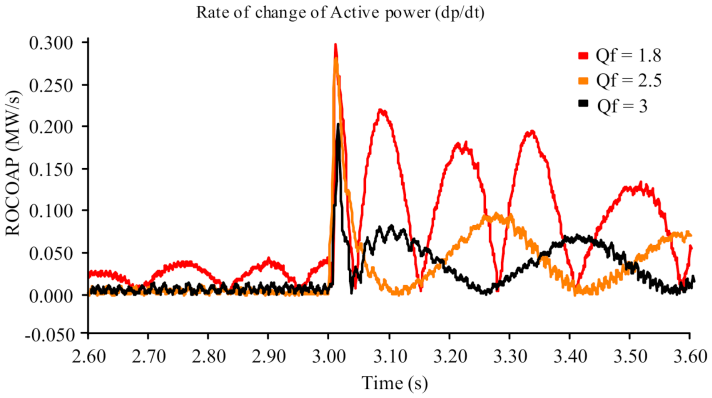


Figure 8. At PCC, DG's ROCOAP (*dp/dt*).

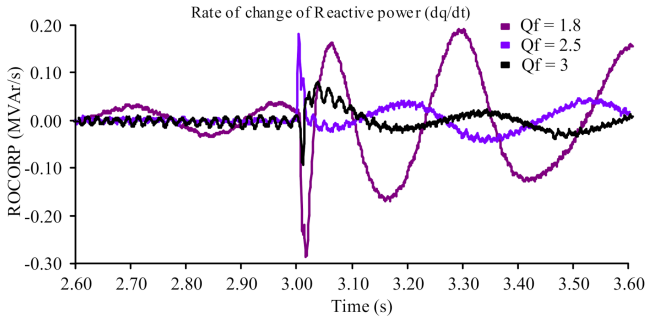


Figure 9. At PCC, DG's ROCORP output (*dq/dt*).

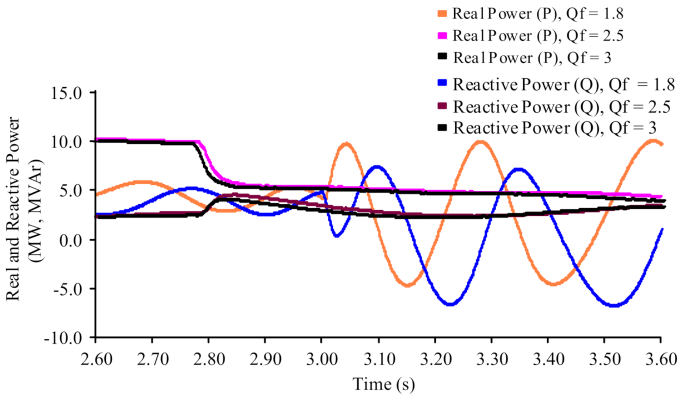


Figure 10. At PCC, DG's real and reactive power.

5.3. Case 3: Initiating the Connection of Varying Reactive Power

For improving the voltage sag and power factor, capacitor banks are connected in parallel with the load, and during this time, the passive parameters of the system change. To check the module performance during the changes in the passive parameters, in this case, different ratings of capacitor banks (1 MVar, 1.5 MVar and 0.5 MVar) are connected at t = 3 s. As can be seen from Figure 11, after connecting the capacitor banks, the ROCOAP value does not cross the maximum margin of 0.7 MW/s. As a result, according to the algorithm, the islanding is correctly rejected for ROCOAP. However, as can be seen from Figure 12, even though ROCORP crosses the threshold, the case is detected as non-islanding by the module, because, according to the algorithm, if ROCOAP does not cross the threshold limit, then the module will not check for the ROCORP condition. This indicates that the proposed IDM is also able to detect non-islanding cases accurately. The proposed IDM results for the selected Q_c are presented in Table 3, and reactive and real power for different Q_c values are shown in Figure 13.

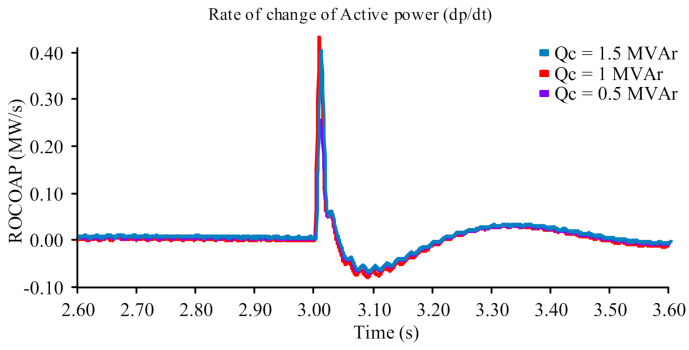


Figure 11. At PCC, DG's ROCOAP (*dp/dt*).

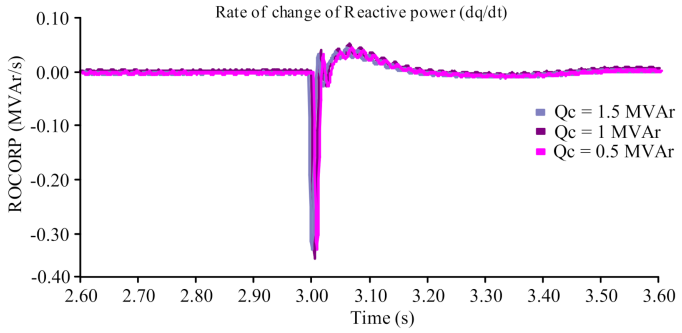


Figure 12. At PCC, DG's ROCORP (*dq*/*dt*).

Table 3. Proposed IDM results for selected Q_c.

Capacitor Switching (Q_c) (MVar)	$\left(\frac{dp_{measured_i}}{dt}\right)$ (MW/s)	$\left(\frac{dq_{measured_i}}{dt}\right)$ (MVar/s)	Time (s)
0.5	0.25	0.03	3–3.04
1	0.43	0.04	3–3.03
1.5	0.40	0.03	3–3.03

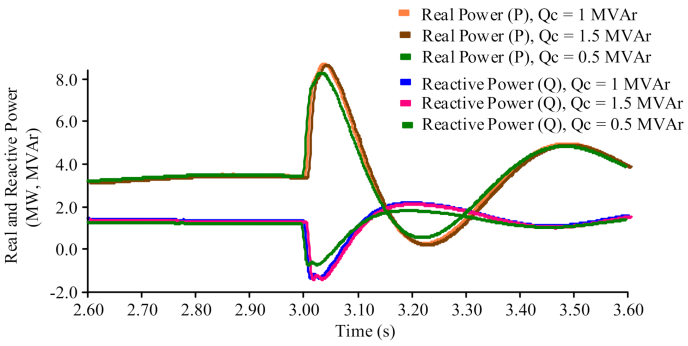


Figure 13. At PCC, DG's real and reactive power.

5.4. Case 4: Fault Analysis

In this section, the performance of the proposed IDM's performance is validated by applying different types of faults. The threshold limits of ROCOAP and ROCORP are set to 0.50 MW/s and 0.1 MVar/s, respectively, during fault conditions. For this case, the load values of active and reactive powers are considered to be 1.1 MW and 0.79 MVar, respectively. The ROCOAP threshold is set to 1 MW/s after connecting the LCS because of the addition of new loads. Under different fault conditions, the detection performances of the proposed IDM are presented in Table 4. Different types of faults (L-G, L-LG, L-L-L-G, and L-L) are applied at the bus 20 Malaysian distribution network at t = 3.02 s. The ROCOAP and ROCORP responses at PCC are shown in Figures 14–17 for fault resistances of 0.01 (Ω) and 0.02 (Ω). From the figures, it can be seen that at t = 3.06 s, the ROCOAP value is more than the threshold 0.50 MW/s. In contrast, the ROCORP value does not exceed the set value of 0.1 MVar/s, because due to the applied fault, the threshold values are changed. Now, according to the proposed algorithm, the LCS started operating and the ROCOAP response during LCS operation is presented in Figures 18 and 19 for fault resistances of 0.01 (Ω) and 0.02 (Ω), respectively. From the figures, it is observed that the ROCOAP value does not exceed the threshold limit of 1 MW/s after connecting the LCS. Since ROCOAP has not exceeded the minimum acceptable limit within the specified period, the system continues to operate by rejecting islanding. The real and reactive power responses of DG units during islanding are depicted in Figure 20.

Table 4. Performance of proposed IDM under different fault conditions.

Fault Type	Resistance (Ω)	$\left(\frac{dp_{measured_i}}{dt}\right)$ (MW/s)	$\left(\frac{dq_{measured_i}}{dt}\right)$ (MVar/s)	$\left(\frac{dp_{measured_i}}{dt}\right)_{LCS}$ (MW/s)
L-L-L-G	0.01	0.69	0.029	0.81
L-L-L-G	0.02	0.71	0.030	0.71
L-L-G	0.01	0.75	0.067	0.85
L-L-G	0.02	0.73	0.068	0.87
L-L	0.01	0.79	0.083	0.93
L-L	0.02	0.79	0.079	0.91
L-G	0.01	0.57	0.061	0.59
L-G	0.02	0.57	0.058	0.63

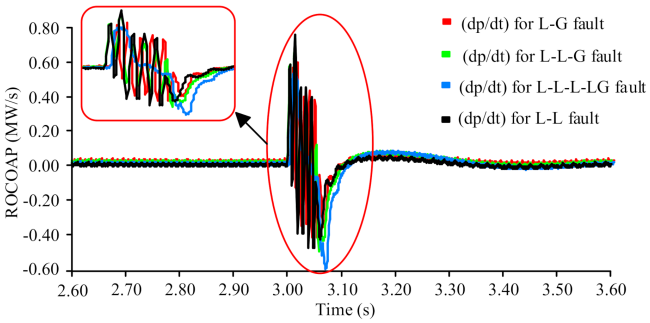


Figure 14. At PCC, DG's ROCOAP (*dp/dt*) for fault resistance 0.01 (Ω).

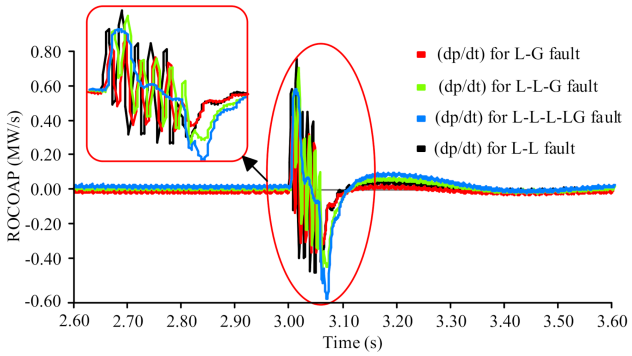


Figure 15. At PCC, DG's ROCOAP (*dp/dt*) for fault resistance 0.02 (Ω).

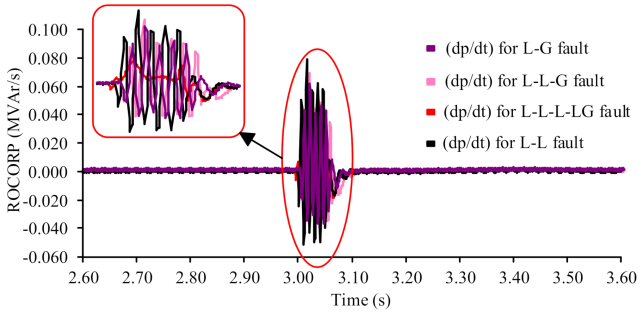


Figure 16. At PCC, DG's ROCORP output (*dq/dt*) for fault resistance 0.01 (Ω).

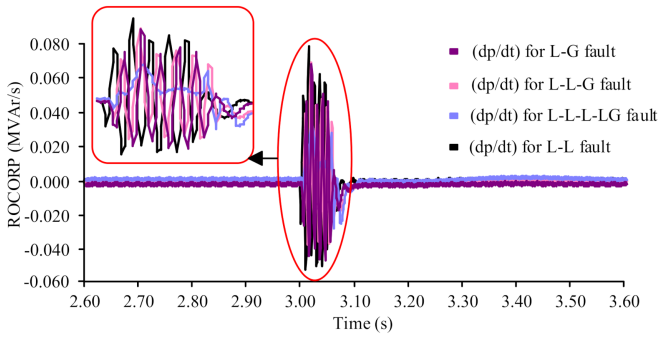


Figure 17. At PCC, DG's ROCORP output (*dq/dt*) for fault resistance 0.02 (Ω).

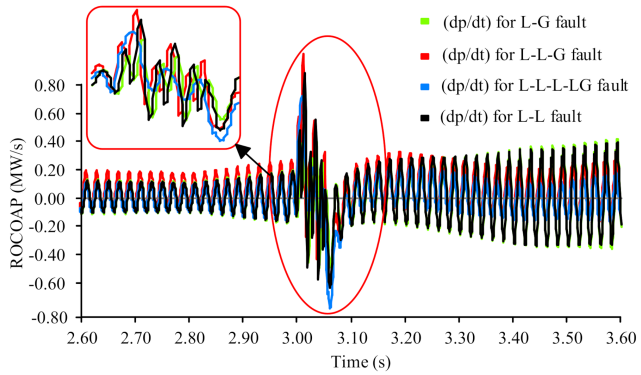


Figure 18. At PCC, DG's ROCOAP (*dp/dt*) after LCS for fault resistance 0.01 (Ω).

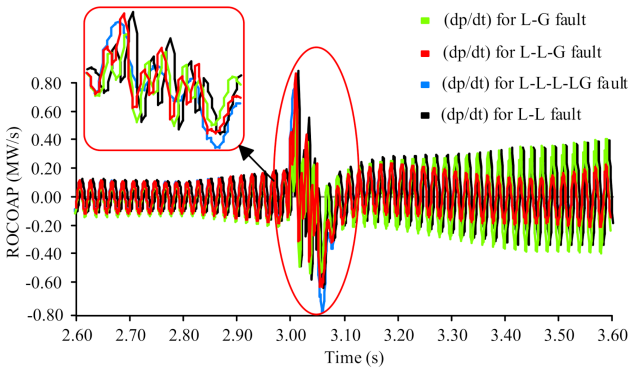


Figure 19. At PCC, DG's ROCOAP (*dp/dt*) after LCS for fault resistance 0.02 (Ω).

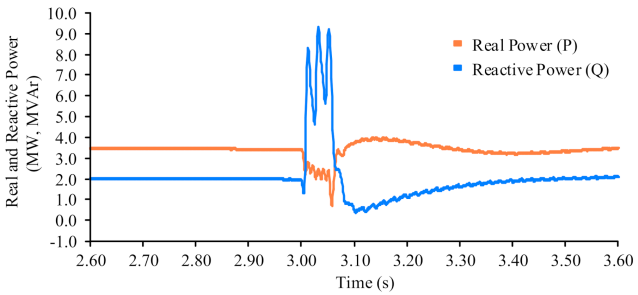


Figure 20. At PCC, DG's real and reactive power.

5.5. Case 5: Starting of Induction Motor

To show that, at the time of induction, the motor starting the module properly perceives the islanding state, in this section, the performance of the proposed IDM is validated by connecting the induction motor at t = 3 s to the network. The ROCOAP and ROCORP threshold values are set to 0.4 MW/s and 0.39 MVar/s, respectively, for this case. The load values of the active and reactive powers are set to 1 MW and 0.8 MVar, respectively.

According to Figure 21, ROCOAP has crossed the threshold of 0.4 MW/s at t = 3 s, whereas the ROCORP value has not crossed the threshold of 0.39 MW/s, which is shown in Figure 22. As a result, the module initiates LCS, and after connecting LCS, it can be seen from Figure 23 that the ROCOAP value has exceeded the threshold limit. On the other hand, after connecting the LCS, ROCORP has not exceeded the threshold of 0.39 MVar/s according to Figure 24, which confirms that the case has accurate non-islanding case detection. Therefore, it is validated that by using the proposed algorithm, non-islanding cases can be detected, and the system continues to work in grid-connected mode with a lagging power factor. DG units' power (real and reactive) responses during islanding are depicted in Figure 25.

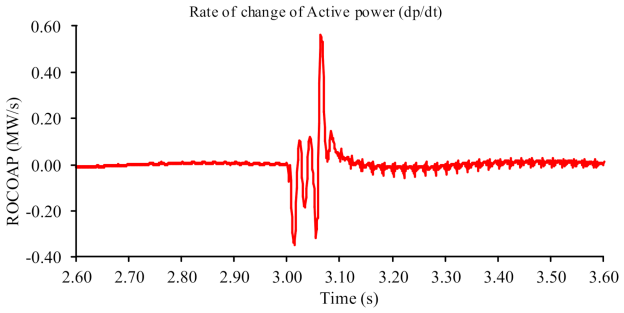


Figure 21. At PCC, DG's ROCOAP (*dp/dt*).

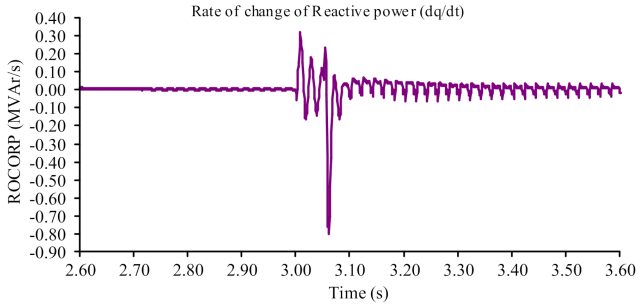


Figure 22. At PCC, DG's ROCORP (*dq/dt*).

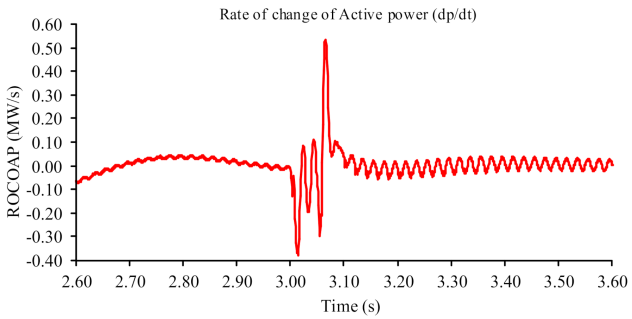


Figure 23. At PCC, DG's ROCOAP (*dp/dt*) after LCS.

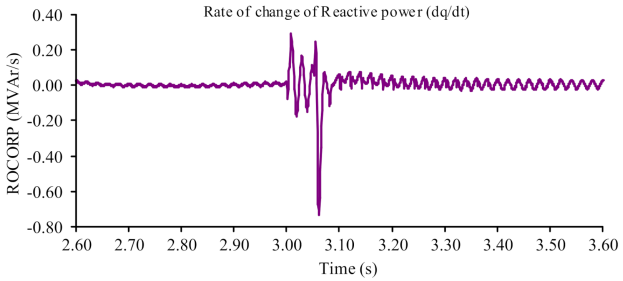


Figure 24. At PCC, DG's ROCORP output (*dq/dt*) after LCS.

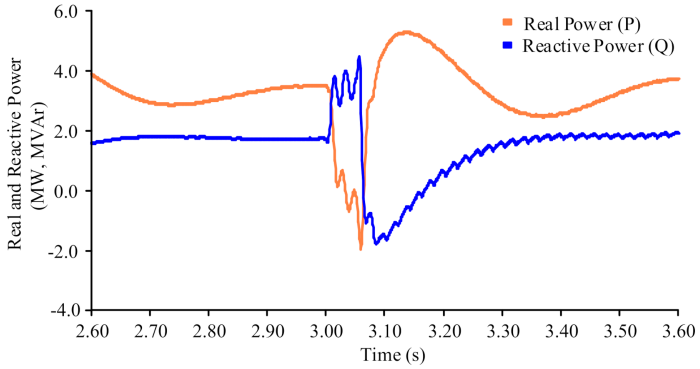


Figure 25. At PCC, DG's real and reactive power.

5.6. Case 6: Zero Power Mismatch

The performances of the proposed IDM are validated during zero active, reactive and total power mismatches in this case study.

5.6.1. Zero Active Power Mismatch

To create a zero active power mismatch scenario, the real power flow between the entire DG systems and the grid is maintained to a zero value at t = 3 s by disconnecting the grid. Figure 26 shows that at t = 3.04 s, the ROCOAP value exceeds the threshold of 0.7 MW/s. As a result, the event is detected as an islanding condition by the module within a three-cycle time period.

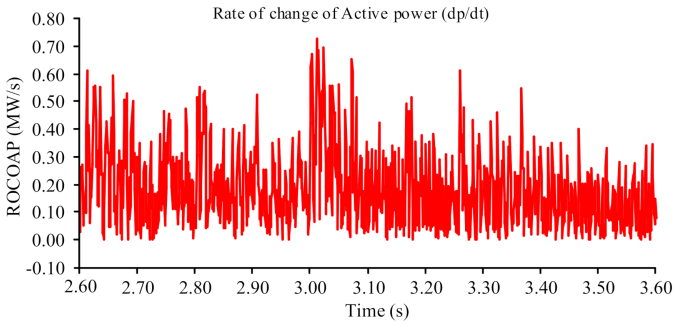


Figure 26. At PCC, DG's ROCOAP (*dp/dt*).

5.6.2. Zero Reactive Power Mismatch

To create a zero active power mismatch scenario, the reactive power flow between the entire DG system and the grid is maintained to a zero value at t = 3 s by disconnecting the grid. Figure 27 shows that at t = 3.04 s, the ROCORP value is 1.2 MVar/s, which exceeds the threshold of 0.08 MVar/s. As a result, islanding conditions are detected accurately by the module and the signals to all DG breakers are sent for disconnection at t = 3.04 s.

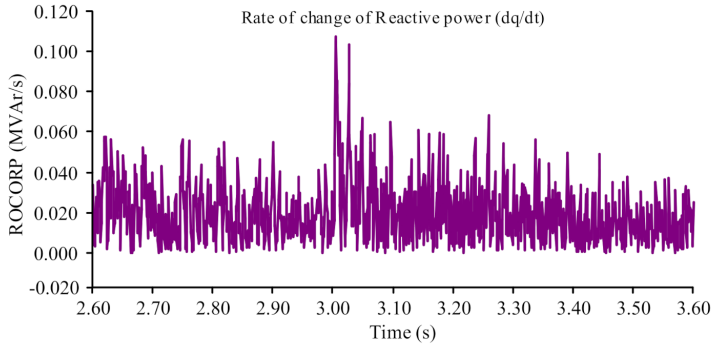


Figure 27. At PCC, DG's ROCORP (*dq/dt*).

5.6.3. Zero Total Power Mismatch

Figure 28 shows that at t= 3.04 s, the value of the rate of change of the total power (ROCOTP) (*dS/dt*) value is 1.4 MVA/s, which has exceeded threshold of 0.08 MVA/s. As a result, islanding conditions are detected accurately by the module and the signals to all DG breakers are sent for disconnection at t = 3.04 s.

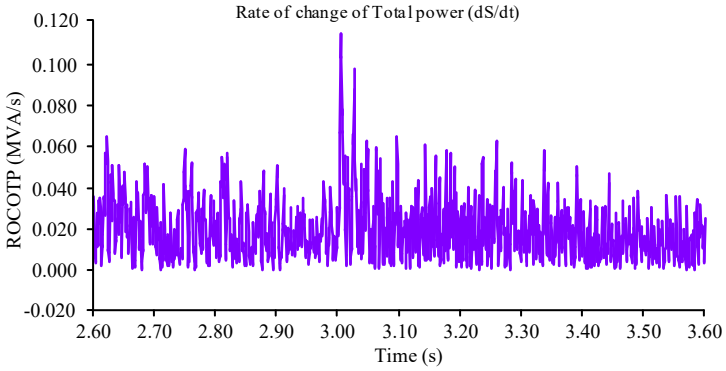


Figure 28. At PCC, DG's ROCOTP (*dS/dt*).

5.7. Case 7: DG Tripping

In the DG-connected distribution system, the tripping of a DG is a very serious issue which can lead to false islanding detection. To verify the performance of the proposed IDM for this case, the PV and biomass are tripped at t = 3 s. For PV and biomass, it is an islanding condition; however, SG is not islanded. From Figure 29, it can be seen that the ROCOAP value increases suddenly up to 0.49 MW/s at t = 3.017 s, but still below the threshold of 0.8 MW/s. As a result, the case is identified as a precise non-islanding case. On the other hand, according to Figure 30, the ROCORP value at t = 3.02 s is found to have exceeded the threshold of 0.019 MVar/s. Even though ROCORP crosses the threshold, the case is detected as non-islanding by the module, because, according to the algorithm, if ROCOAP does not cross the threshold limit, the module will not check for ROCORP. This indicates that the proposed IDM is able to detect both islanding and non-islanding cases accurately.

5.8. Comparison with Previous Islanding Detection Methods

5.8.1. Based on Islanding Detection Time

In this section, the proposed IDM performance is compared with the other hybrid methods in [36,41–43] based on the detection time, which is presented in Table 5. From the table, it can be seen that the combined voltage and reactive power shift IDM [36] took 160 ms to detect islanding. On the other hand, the ROCOF and ROCORP combined IDM [41], similar to the proposed method, has a detection time of 200 ms, which is higher than the proposed method. The combination of a ROCOV and ROCORP-based hybrid

IDM [42] has a detection time of 250 ms, which is higher than both the proposed method and the method in [41]. Finally, it is observed that the ROCORV and ROCORP combined hybrid IDM [43] has a longer detection time (640 ms) than previous methods. From the above discussion, it is clear that even though all the hybrid IDMs were able to detect the islanding within 2 s, which satisfies the IEEE 1547 standards, the proposed hybrid IDM's detection time is faster than others.

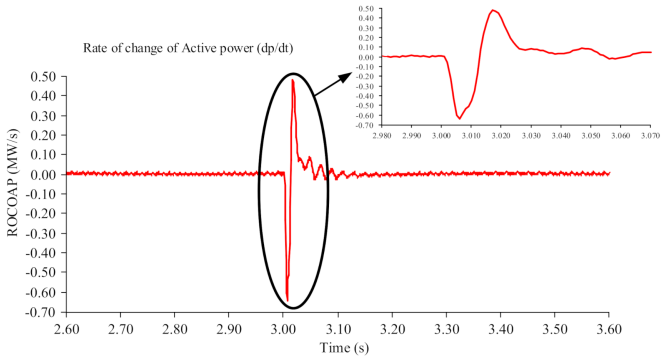


Figure 29. At PCC, DG's ROCOAP (*dp/dt*).

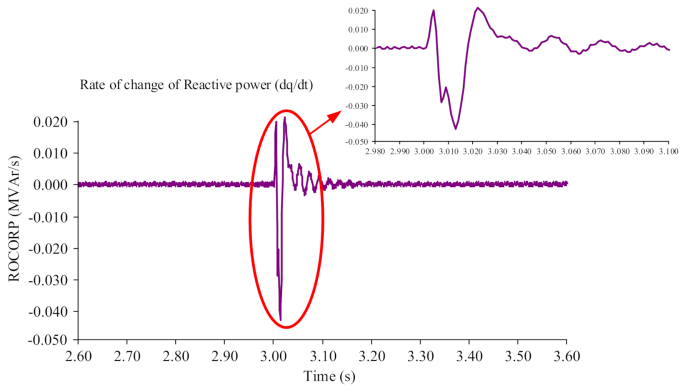


Figure 30. At PCC, DG's ROCORP output (*dq/dt*).

Table 5. Comparison of different IDMs based on islanding detection time.

Hybrid Islanding Detection Methods	Islanding Detection Time
Proposed method	90 ms (5 cycles)
Voltage and Reactive Power Shift [36]	160 ms (8 cycles)
ROCOF over ROCORP (df/dq) [41]	200 ms (10 cycles)
ROCOV and ROCORP [42]	250 ms (15 cycles)
ROCORV over ROCORP (dE/dq) [43]	640 ms (32 cycles)

5.8.2. Based on NDZ

In this section, the proposed method's performance is compared with other hybrid IDMs [36,41–43] based on the NDZ that is presented in Table 6. The comparison results of different IDMs based on only NDZ is presented in Figure 31. From Figure 31, it can be seen that the proposed IDM has a smaller NDZ in comparison with other IDMs, and islanding is recognized satisfactorily using the proposed hybrid IDM. Further, the proposed IDM is not negatively influenced by any kinds of faults.

Table 6. Comparison of proposed method with other IDM techniques.

Methods	NDZ
Proposed method	$-5\% \leq \frac{\Delta P}{P} \leq 4.3\%$
	$-4.5\% \leq \frac{\Delta Q}{Q} \leq 4.3\%$
Ref [36]	$-45\% \leq \frac{\Delta P}{P} \leq 38.41\%$
	$-18\% \leq \frac{\Delta Q}{Q} \leq 17\%$
Ref [41]	$-5\% \leq \frac{\Delta P}{P} \leq 5\%$
	$-5\% \leq \frac{\Delta Q}{Q} \leq 5\%$
Ref [42]	$-6\% \leq \frac{\Delta P}{P} \leq 6\%$
	$-12\% \leq \frac{\Delta Q}{Q} \leq 11.8\%$
Ref [43]	$-25\% \leq \frac{\Delta P}{P} \leq 22\%$
	$-11\% \leq \frac{\Delta Q}{Q} \leq 11\%$

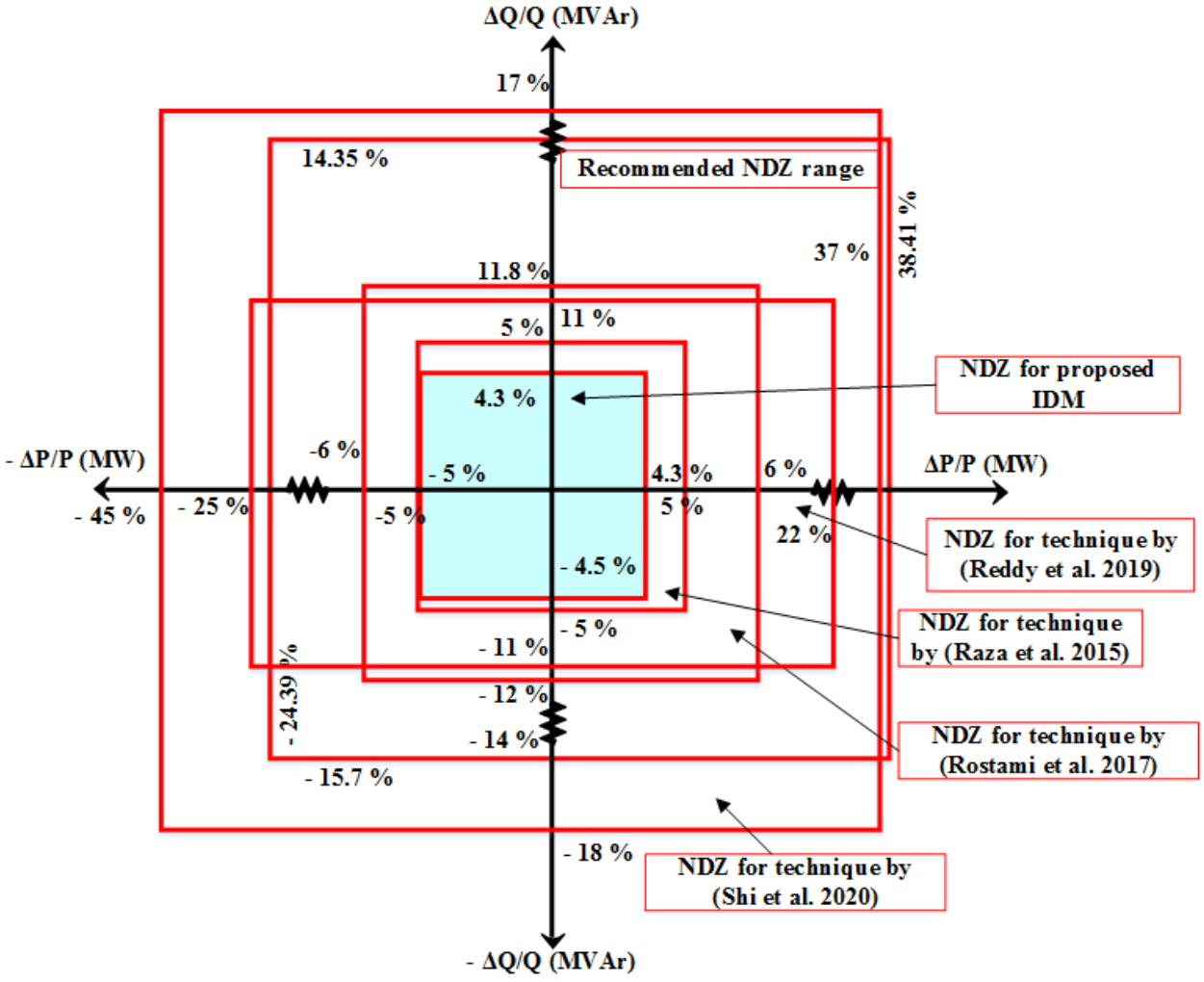


Figure 31. NDZ comparison of the proposed IDM with different hybrid IDMs.

6. Conclusions

This work has presented a novel hybrid IDM based on the estimation of power changes and load fluctuation in the distribution system. The performance of the proposed IDM has validated for different islanding and non-islanding cases in the PSCAD/EMTDC platform,

whereas a testbed Malaysian distribution network (11 kV) has also been considered. From the simulation results, the efficacy of the proposed IDM is perceived because within 0.09 s, the proposed IDM was able to detect islanding, which is lower than 2 s, which is in line with the IEEE standard 1547. In addition, for a distribution network consisting of multiple and different DGs (SG, PV and biomass), the proposed IDM has also shown excellent performance by successfully differentiating between islanding and non-islanding cases.

A comparative study based on the detection period between the proposed IDM and three different hybrid detection methods to prove the better performance of the proposed method has been carried out in this paper. It can be seen that the detection time taken by the proposed IDM is 0.09 s, which is 0.07 s, 0.11 s, 0.16 s and 0.55 s less than the other hybrid IDMs, namely the combined voltage and reactive power shift IDM, ROCOF and ROCORP IDM, ROCOV and ROCORP IDM, and ROCORV and ROCORP IDM, respectively. Furthermore, it is observed that the proposed IDM has a smaller NDZ compared to other available hybrid IDMs.

In this work, through simulation only the performance of the proposed IDM has been validated in an existing Malaysian network. Therefore, to prove its effectivity also in real-world conditions in the future, the performance of the proposed IDM module will be verified through either hardware-in-loop simulations or hardware implementation.

Author Contributions: Conceptualization, methodology, and simulation, U.K.J. and S.A.; manuscript writing and editing, U.K.J., S.A. and T.A. All authors have read and agreed to the published version of the manuscript.

Funding: The authors would like to thank University of Malaya, Malaysia and Chittagong University of Engineering and Technology, Chittagong, Bangladesh for providing research facilities.

Data Availability Statement: The data used in this research is enclosed within the manuscript. No external data sources are used in this research.

Conflicts of Interest: The authors declare no conflict of interest.

Abbreviations

DG	Distributed Generator
IEEE	Institute of Electrical and Electronics Engineers
PCC	Point of Common Coupling
NDZ	Non-Detection Zone
SFS	Sandia Frequency Shift
PMU	Phasor Measurement Units
ROCOF	Rate of change frequency
ROCOAP	Rate of change of active power
ROCOV	Rate of change of voltage
ANN	Artificial Neural Network
PSCAD	Power System Computer Aided Design
PV	Photovoltaic
ANFIS	Adaptive Neuro-Fuzzy Inference System
IEC	International Electrotechnical Commission
PLL	Phase Lock Loop
IDM	Islanding Detection Method
PLC	Power Line Carrier
ROCOP	Rate of change of Power
ROCORP	Rate of change of reactive power
LCS	Load Connecting Strategy
ROCORV	Rate of change of regulator voltage
SVM	Support Vector Machine
SG	Synchronous Generator
CB	Circuit Breaker

Appendix A

Table A1. Malaysian distribution network (11 kV) parameters [57].

System Parameter	Value
Voltage of grid	132 kV
Power capacity grid	10 MVA
Frequency of grid	50 Hz
Rated power of grid transformer	50 MVA
Voltage of Transformer (step-up)	3.3/11 kV
Voltage of Transformer (step-down)	132/11 kV
L_s	1 mH
R_s	1 Ω
Rated power of DG transformer	2 MVA
Load voltage	11kV
Synchronous generator rating	1.8 MW
PV generation	1 MW
Biomass Generator	0.8 MW

Table A2. Malaysian distribution network (11 kV) load data [57].

Load Bus	$\text{Load}_{\text{Active Power}}$ (MW)	$\text{Load}_{\text{Reactive Power}}$ (MVar)
1	0.45	0.198
2	0.06645	0.039
3	0.061128	0.0378
4	0.36	0.126
5	0.232668	0.12
6	0.160716	0.09957
7	0.1948	0.09165
8	0.187557	0.11631
9	0.057213	0.035676
10	0.013548	0.009957
11	0.014025	0.008763
12	0.3	0.126
13	0.125454	0.075
14	0.062163	0.0384
15	0.051252	0.0375
16	0.074061	0.045
17	0.05262	0.033
18	0.151419	0.105
19	0.12918	0.0801
20	0.272244	0.1926
21	0.094762	0.04731
22	0.207957	0.10872
23	0.084666	0.0516

Table A2. *Cont.*

Load Bus	$\text{Load}_{\text{Active Power}}$ (MW)	$\text{Load}_{\text{Reactive Power}}$ (MVar)
24	0.076044	0.0462
25	0.318322	0.129
26	0.179049	0.111
27	0.178356	0.108
28	0.241703	0.066

References

1. Barzkar, A.; Hosseini, S.M.H. A novel peak load shaving algorithm via real-time battery scheduling for residential distributed energy storage systems. *Int. J. Energy Res.* **2018**, *42*, 2400–2416. [CrossRef]
2. Bajaj, M.; Singh, A.K. Grid integrated renewable DG systems: A review of power quality challenges and state-of-the-art mitigation techniques. *Int. J. Energy Res.* **2020**, *44*, 26–69. [CrossRef]
3. IEEE Standards Association. *IEEE 1547 Standard for Interconnecting Distributed Resources with Electric Power Systems*; IEEE Standards Association: Piscataway, NJ, USA, 2003.
4. Narang, D. IEEE Standard for Interconnection and Interoperability of Distributed Energy Resources with Associated Electric Power Systems Interfaces. In *IEEE Std 1547-2018 (Revision of IEEE Std 1547-2003)*; IEEE Standards Association: Piscataway, NJ, USA, 2018.
5. International Electrotechnical Commission. *IEC 62116 ED3 Utility-Interconnected Photovoltaic Inverters—Test Procedure of Islanding Prevention Measures*. 2014. Available online: https://www.iec.ch/dyn/www/f?p=103:38:614853414433067::::FSP_ORG_ID,FSP_APEX_PAGE,FSP_PROJECT_ID:1276,23,107275 (accessed on 7 October 2021).
6. Khan, M.A.; Haque, A.; Kurukuru, V.B.; Saad, M. Islanding detection techniques for grid-connected photovoltaic systems—A review. *Renew. Sustain. Energy Rev.* **2022**, *154*, 111854. [CrossRef]
7. Islam, M.M.; Nagrial, M.; Rizk, J.; Hellany, A. General Aspects, Islanding Detection, and Energy Management in Microgrids: A Review. *Sustainability* **2021**, *13*, 9301. [CrossRef]
8. Abokhalil, A.G.; Awan, A.B.; Al-Qawasmi, A.R. Comparative study of passive and active islanding detection methods for PV grid-connected systems. *Sustainability* **2018**, *10*, 1798. [CrossRef]
9. Inverters, Converters, Controllers and Interconnection System Equipment for Use with Distributed Energy Resources. Standard UL-1741. 2010. Available online: https://scholar.google.com/scholar?hl=en&as_sdt=0%2C5&q=9.%09Inverters%2C+Converters%2C+Controllers+and+Interconnection+System+Equipment+for+Use+with+Distributed+Energy+Resources++.+Standard+UL-1741.+2010++.&btnG= (accessed on 7 October 2021).
10. Photovoltaic. IEEE 929-2000 Systems, Recommended Practice for Utility Interconnected Photovoltaic. 2000. Available online: https://ieeexplore.ieee.org/document/836389 (accessed on 7 October 2021).
11. Teodorescu, R.; Liserre, M.; Rodriguez, P. *Grid Converters for Photovoltaic and Wind Power Systems*; John Wiley & Sons: Chichester, UK, 2011; Volume 29.
12. Hongesombut, K.; Punyakunlaset, S.; Romphochai, S. Under Frequency Protection Enhancement of an Islanded Active Distribution Network Using a Virtual Inertia-Controlled-Battery Energy Storage System. *Sustainability* **2021**, *13*, 484. [CrossRef]
13. Menon, V.; Nehrir, M.H. A hybrid islanding detection technique using voltage unbalance and frequency set point. *IEEE Trans. Power Syst.* **2007**, *22*, 442–448. [CrossRef]
14. Perlenfein, S.; Ropp, M.; Neely, J.; Gonzalez, S.; Rashkin, L. Subharmonic power line carrier (PLC) based island detection. In Proceedings of the 2015 IEEE Applied Power Electronics Conference and Exposition (APEC), Charlotte, NC, USA, 15–19 March 2015; pp. 2230–2236.
15. Xu, W.; Zhang, G.; Li, C.; Wang, W.; Wang, G.; Kliber, J. A power line signaling based technique for anti-islanding protection of distributed generators—Part I: Scheme and analysis. *IEEE Trans. Power Deliv.* **2007**, *22*, 1758–1766. [CrossRef]
16. Zhang, Y.; Xu, Y.; Dong, Z.Y. Robust ensemble data analytics for incomplete PMU measurements-based power system stability assessment. *IEEE Trans. Power Syst.* **2017**, *33*, 1124–1126. [CrossRef]
17. Wang, S.; Dehghanian, P.; Li, L. Power grid online surveillance through PMU-embedded convolutional neural networks. *IEEE Trans. Ind. Appl.* **2019**, *56*, 1146–1155. [CrossRef]
18. Naradon, C.; Chai, C.I.; Leelajindakrairerk, M.; Chow, C.I. A case study on the interoperability of the Direct Transfer Trip (DTT) technique with carrier signal protection schemes (PTT and DEF) and SCADA system between two utilities in Thailand. In Proceedings of the 2017 IEEE International Conference on Environment and Electrical Engineering and 2017 IEEE Industrial and Commercial Power Systems Europe (EEEIC/I & CPS Europe), Milan, Italy, 6–9 June 2017; pp. 1–7.
19. Murugesan, S.; Murali, V.; Daniel, S.A. Hybrid analyzing technique for active islanding detection based on d-axis current injection. *IEEE Syst. J.* **2017**, *12*, 3608–3617. [CrossRef]
20. Wen, B.; Boroyevich, D.; Burgos, R.; Shen, Z.; Mattavelli, P. Impedance-based analysis of active frequency drift islanding detection for grid-tied inverter system. *IEEE Trans. Ind. Appl.* **2015**, *52*, 332–341. [CrossRef]

21. Trujillo, C.L.; Velasco, D.; Figueres, E.; Garcerá, G. Analysis of active islanding detection methods for grid-connected microinverters for renewable energy processing. *Appl. Energy* **2010**, *87*, 3591–3605. [CrossRef]
22. Jia, K.; Xuan, Z.; Lin, Y. An islanding detection method for grid-connected photovoltaic power system based on Adaboost algorithm. *Trans. China Electrotechn. Soc.* **2018**, *33*, 1106–1113.
23. Mohammadpour, B.; Zareie, M.; Eren, S.; Pahlevani, M. Stability analysis of the slip mode frequency shift islanding detection in single phase PV inverters. In Proceedings of the 2017 IEEE 26th International Symposium on Industrial Electronics (ISIE), Edinburgh, UK, 19–21 June 2017; pp. 873–878.
24. Hatata, A.Y.; Abd-Raboh, E.H.; Sedhom, B.E. Proposed Sandia frequency shift for anti-islanding detection method based on artificial immune system. *Alex. Eng. J.* **2018**, *57*, 235–245. [CrossRef]
25. Vazquez, E.; Vazquez, N.; Femat, R. Modified Sandia voltage shift anti-islanding scheme for distributed power generator systems. *IET Power Electron.* **2020**, *13*, 4226–4234. [CrossRef]
26. Galleani, L.; Tavella, P. Robust detection of fast and slow frequency jumps of atomic clocks. *IEEE Trans. Ultrason. Ferroelectr. Freq. Control* **2016**, *64*, 475–485. [CrossRef]
27. Chiang, W.J.; Jou, H.L.; Wu, J.C. Active islanding detection method for inverter-based distribution generation power system. *Int. J. Electr. Power Energy Syst.* **2012**, *42*, 158–166. [CrossRef]
28. Bakhshi, M.; Noroozian, R.; Gharehpetian, G.B. Novel islanding detection method for multiple DGs based on forced Helmholtz oscillator. *IEEE Trans. Smart Grid* **2017**, *9*, 6448–6460. [CrossRef]
29. Abd-Elkader, A.G.; Saleh, S.M.; Eiteba, M.M. A passive islanding detection strategy for multi-distributed generations. *Int. J. Electr. Power Energy Syst.* **2018**, *99*, 146–155. [CrossRef]
30. Gupta, P.; Bhatia, R.S.; Jain, D.K. Average absolute frequency deviation value based active islanding detection technique. *IEEE Trans. Smart Grid* **2014**, *6*, 26–35. [CrossRef]
31. Reddy, V.R.; Sreeraj, E.S. A feedback-based passive islanding detection technique for one-cycle-controlled single-phase inverter used in photovoltaic systems. *IEEE Trans. Ind. Electron.* **2019**, *67*, 6541–6549. [CrossRef]
32. Xie, X.; Huang, C.; Li, D. A new passive islanding detection approach considering the dynamic behavior of load in microgrid. *Int. J. Electr. Power Energy Syst.* **2020**, *117*, 105619. [CrossRef]
33. Makwana, Y.M.; Bhalja, B.R. Experimental performance of an islanding detection scheme based on modal components. *IEEE Trans. Smart Grid* **2017**, *10*, 1025–1035. [CrossRef]
34. Rabuzin, T.; Hohn, F.; Nordström, L. Computation of sensitivity-based islanding detection parameters for synchronous generators. *Electr. Power Syst. Res.* **2021**, *190*, 106611. [CrossRef]
35. Ambia, M.N.; Al-Durra, A.; Caruana, C.; Muyeen, S.M. Islanding operation of hybrid microgrids with high integration of wind driven cage induction generators. *Sustain. Energy Technol. Assess.* **2016**, *13*, 68–75. [CrossRef]
36. Shi, K.; Ye, H.; Xu, P.; Yang, Y.; Blaabjerg, F. An islanding detection based on droop characteristic for virtual synchronous generator. *Int. J. Electr. Power Energy Syst.* **2020**, *23*, 106277. [CrossRef]
37. Sirjani, R.; Okwose, C.F. Combining two techniques to develop a novel islanding detection method for distributed generation units. *Measurement* **2016**, *81*, 66–79. [CrossRef]
38. Nayak, A.M.; Mishra, M.; Pati, B.B. A Hybrid Islanding Detection Method Considering Voltage Unbalance Factor. In Proceedings of the 2020 IEEE International Symposium on Sustainable Energy, Signal Processing and Cyber Security (iSSSC), Gunupur Odisha, India, 16–17 December 2020; pp. 1–5.
39. Khodaparastan, M.; Vahedi, H.; Khazaeli, F.; Oraee, H. A novel hybrid islanding detection method for inverter-based DGs using SFS and ROCOF. *IEEE Trans. Power Deliv.* **2015**, *32*, 2162–2170. [CrossRef]
40. Laghari, J.A.; Mokhlis, H.; Bakar AH, A.; Karimi, M. A new islanding detection technique for multiple mini hydro based on rate of change of reactive power and load connecting strategy. *Energy Convers. Manag.* **2013**, *76*, 215–224. [CrossRef]
41. Raza, S.; Mokhlis, H.; Arof, H.; Laghari, J.A.; Mohamad, H. A sensitivity analysis of different power system parameters on islanding detection. *IEEE Trans. Sustain. Energy* **2015**, *7*, 461–470. [CrossRef]
42. Rostami, A.; Abdi, H.; Moradi, M.; Olamaei, J.; Naderi, E. Islanding detection based on ROCOV and ROCORP parameters in the presence of synchronous DG applying the capacitor connection strategy. *Electr. Power Compon. Syst.* **2017**, *45*, 315–330. [CrossRef]
43. Reddy, C.R.; Reddy, K.H. A new passive islanding detection technique for integrated distributed generation system using rate of change of regulator voltage over reactive power at balanced islanding. *J. Electr. Eng. Technol.* **2019**, *14*, 527–534. [CrossRef]
44. Kumar, D. Islanding Detection in Microgrid Compromising Missing Values Using NI Sensors. *IEEE Syst. J.* **2021**, 1–10, *Early Access*. Available online: https://ieeexplore.ieee.org/abstract/document/9363448?casa_token=OfmzxBe9eVsAAAAA:6vl8nJ4kTC4i_Tml3gTNrvHLJfs2BoiJHEzKTwPJbOB-2WDibgsAPu13nwTI_nrzt9kQ-HpL (accessed on 7 October 2021). [CrossRef]
45. Mlakić, D.; Baghaee, H.R.; Nikolovski, S. A novel ANFIS-based islanding detection for inverter-interfaced microgrids. *IEEE Trans. Smart Grid* **2018**, *10*, 4411–4424. [CrossRef]
46. Khan, M.A.; Kurukuru, V.B.; Haque, A.; Mekhilef, S. Islanding Classification Mechanism for Grid-Connected Photovoltaic Systems. *IEEE J. Emerg. Sel. Top. Power Electron.* **2020**, *9*, 1966–1975. [CrossRef]
47. Khan, M.A.; Haque, A.; Kurukuru, V.S.B. Machine learning based islanding detection for grid connected photovoltaic system. In Proceedings of the 2019 International Conference on Power Electronics, Control and Automation (ICPECA), New Delhi, India, 16–17 November 2019; pp. 1–6.

48. Khan, M.A.; Haque, A.; Kurukuru, V.S.B. An Efficient Islanding Classification Technique for Single Phase Grid Connected Photovoltaic System. In Proceedings of the 2019 International Conference on Computer and Information Sciences (ICCIS), Sakaka, Saudi Arabia, 3–4 April 2019; pp. 1–6.
49. Paiva, S.C.; de Araujo Ribeiro, R.L.; Alves, D.K.; Costa, F.B.; Rocha TD, O.A. A wavelet-based hybrid islanding detection system applied for distributed generators interconnected to AC microgrids. *Int. J. Electr. Power Energy Syst.* **2020**, *121*, 106032. [CrossRef]
50. Ahmadipour, M.; Hizam, H.; Othman, M.L.; Radzi MA, M.; Chireh, N. A novel islanding detection technique using modified Slantlet transform in multi-distributed generation. *Int. J. Electr. Power Energy Syst.* **2019**, *112*, 460–475. [CrossRef]
51. Menezes, T.S.; Fernandes, R.A.; Coury, D.V. Intelligent islanding detection with grid topology adaptation and minimum non-detection zone. *Electr. Power Syst. Res.* **2020**, *187*, 106470. [CrossRef]
52. Farhan, M.A. Mathematical morphology-based islanding detection for distributed generation. *IET Gener. Transm. Distrib.* **2017**, *11*, 3449–3457. [CrossRef]
53. Chaitanya, B.K.; Yadav, A. Hilbert–huang transform based islanding detection scheme for distributed generation. In Proceedings of the 2018 IEEE 8th Power India International Conference (PIICON), Kurukshetra, India, 10–12 December 2018; pp. 1–5.
54. Guo, Y.; Li, K.; Laverty, M.; Xue, Y. Synchrophasor-based islanding detection for distributed generation systems using systematic principal component analysis approaches. *IEEE Trans. Power Deliv.* **2015**, *30*, 2544–2552. [CrossRef]
55. Padhee, M.; Dash, P.K.; Krishnanand, K.R.; Rout, P.K. A fast Gauss-Newton algorithm for islanding detection in distributed generation. *IEEE Trans. Smart Grid* **2012**, *3*, 1181–1191. [CrossRef]
56. Kolli, A.T.; Ghaffarzadeh, N. A novel phaselet-based approach for islanding detection in inverter-based distributed generation systems. *Electr. Power Syst. Res.* **2020**, *182*, 106226. [CrossRef]
57. Jhuma, U.K.; Mekhilef, S.; Mubin, M.; Ahmad, S.; Alturki, Y. Hybrid islanding detection technique for distribution network considering the dynamic behavior of power and load. *Int. J. Circuit Theory Appl.* **2021**. [CrossRef]
58. Islam, H.; Mekhilef, S.; Shah, N.M.; Soon, T.K.; Wahyudie, A.; Ahmed, M. Improved Proportional-Integral Coordinated MPPT Controller with Fast Tracking Speed for Grid-Tied PV Systems under Partially Shaded Conditions. *Sustainability* **2021**, *13*, 830. [CrossRef]
59. Alturki, F.A.; Awwad, E.M. Sizing and cost minimization of standalone hybrid wt/pv/biomass/pump-hydro storage-based energy systems. *Energies* **2021**, *14*, 489. [CrossRef]